Reduced interaction between numerical and model errors through anisotropic filtering

Marcello Meldi and Federico Perini

Dipartimento di Ingegneria Meccanica e Civile, Università di Modena, Italy.
marcello.meldi@unimore.it federico.perini@unimore.it

Summary. The work addresses to a better comprehension of the error assessment in LES due to the coupling between the model and the numerical discretisation.
The possibility to reduce the interactions between the error sources is investigated on different test cases through the use of an algebraic function correlating the subfilter and subgrid wavelengths, respectively $\bar{\Delta}$ and Δ, incrementing the ratio between the two where the scales are poorly resolved.
The analysis, considering a range of grid resolutions as well as subfilter models, has been performed starting from database sets which have been reconstructed with ordinary kriging to estimate the sensitiveness of the strategy with respect to the simulation parameters. The results indicate that a reduction in the error cost function can be achieved for most subfilter models and that the approach looks quite stable for a moderate range of the grid resolution.

Key words: Large-eddy Simulation, anisotropic filtering, errors interaction

1 Introduction

The main concern regarding LES in industrial applications is the definition of criteria for the error assessment, as the increasing computational resources make LES an operable tool to the simulation of High-Reynolds complex flows.
In *traditional* LES the filtering operator is performed by the grid discretisation: the scales smaller than the geometric wavelength Δ are not captured by the simulation and are defined as *subgrid scales*.
While Δ is actually straightforward defined on structured isotropic grids, its definition may be arguable when dealing with anisotropic or unstructured grids, as in most industrial applications.
The problem has been approached by many authors in different ways ([1], [2]) but all the proposals till now presented about this topic focus on the geometry and do not take into account the flow behaviour.
The model used to close the set of equations acts as a filter too, introducing a

second wavelength $\bar{\Delta}$: the scales filtered by the model will be hereafter indicated as *subfilter scales* [3]. The way these two filters interact is of difficult comprehension as the shape of the resulting filter kernels is extremely case sensitive: this may lead to unpredictable behaviour due to strongly non-linear error dynamics. Furthermore Ghosal [4] showed that the numerical error is of the same order of the modelling error for most of the wave numbers and proposed as a possible solution the combination of prefiltering and high order schemes. Since this approach increases noticeably the computational cost and the complexity of the problem, a more common solution is to increase the ratio $\bar{\Delta}/\Delta$ to force the error dynamics to be governed by the model error. A high ratio can be achieved either by improving the grid resolution or by extending the filter width, but the application of these guidelines on the whole domain may anyway produce inadequate results, in terms of significantly increased computational costs or lack of resolution. As the interactions between numerical and model errors are particularly strong in the smallest resolved scales, the main idea of our work is a local increase of $\bar{\Delta}$ extending it only where needed. This kind of approach should modify the model filter kernel as to reduce the interaction between the 2 main sources of error and produce a lower discretisation dependence of the error itself.
This approach has been intensively tested to check its robustness when coupled with different subgrid-scales models, numerical discretisations or grids.
The paper is structured as follows: in section 2 LES and filtering approaches are presented as well as an exhaustive explanation of the *universal anisotropic* $\bar{\Delta}$ (UAD) approach is furnished. The main results by the application of the anisotropic $\bar{\Delta}$ to two different test cases are summed up in section 3, while in the last section 4 conclusions are drawn.

2 Theoretical LES

2.1 The filtering operation

We consider here Newtonian, incompressible, three-dimensional and time-dependent flows.The scales separation in LES is achieved by the application of a scale high-pass filter, which is mathematically formulated as a convolution product in the physical space. The Fourier transform of the filter kernel G is associated to a bandwidth length $\bar{\Delta}$ that separates the resolved scales from the filtered ones, which are not directly solved but modelled adding the τ_{LES} closure term to the momentum equation.

2.2 LES Models

In the following analysis four different models have been tested to check their sensitiveness to the application of the UAD filtering approach. The model chosen are the One-equation Turbulent Energy Model [5], the Smagorinsky

Model [6], the Variational multi-scale approach [7] applied to the Smagorinsky one and the WALE model [8].
It is actually useful to remark that, as each model relate in a different way the ν_{LES} with $\bar{\Delta}$, we can expect that the overall results will be sensitive of the different coupling between model and UAD. In the following sections, the models will be respectively refereed ans ONE, SM, VMS and $WALE$.

2.3 UAD Approach

This paper focuses on the possibility to mask the numerical error by means of the model one, as it generally looks like that $\bar{\Delta}/\Delta > 1$ is beneficial for pursuing a global error reduction and the application of a $\bar{\Delta}$ significantly higher than the Δ produces grid-independent numerical solutions [9].
A high ratio value is not anyway necessary on the whole physical domain, but just locally where the numerical error becomes large if compared to the model error, a situation most common when estimating the resolution of the smallest resolved scales. The strategy we are proposing relies indeed on the possibility to extend the subfilter wavelength $\bar{\Delta}$ only where the scales are poorly resolved through the definition of an algebraic function relating $\bar{\Delta}$ and Δ:

$$f_{UAD} = \frac{\bar{\Delta}_{UAD}}{\Delta} = 1 + C_{UAD}\ \Theta\ \tanh(\Psi)^{\frac{1}{\Theta}} \tag{1}$$

Θ and Ψ are respectively a parameter estimating the global and local resolution, while C_{UAD} is a constant. The shape of the function f_{UAD} for a value of $C_{UAD} = 5$ is presented in figure 1(a).
The parameter Ψ is an indicator of the wavelength of the resolved scales: as the parameter increases, smaller scales are locally present. Since vorticity is a quantity which clearly indicates the presence of small scales, we decided to define the parameter Ψ as the normalised magnitude of the vorticity vector

$$\Psi = \sqrt[4]{\frac{\omega}{\max(\omega)}} \tag{2}$$

the fourth root of Ψ being chosen as in that condition UAD results less case sensitive and a greater part of the volume is affected by the anisotropic filtering, fig. 1(b).
While the parameter Ψ is a field parameter, i.e. every computational cell has its own Ψ value, the parameter Θ is a scalar indicating the global resolution of the system, and his value determines the shape and the intensity of the function f_{UAD}. The form factor Θ, defined by the eq. 3, shapes the curve tending to flatten it out when vorticity increases (which is the case of well-resolved LES) while ensures a strong effect on most of the scales when the field is poorly resolved, as from picture 1(a).

$$\Theta = \frac{2 < \bar{U} >^2}{< \bar{U} >^2 + l^2 < \omega >^2} \tag{3}$$

l is taken as twice the characteristic length of the test case and $\bar{U}$ is the velocity magnitude .<> denotes a spatial average.

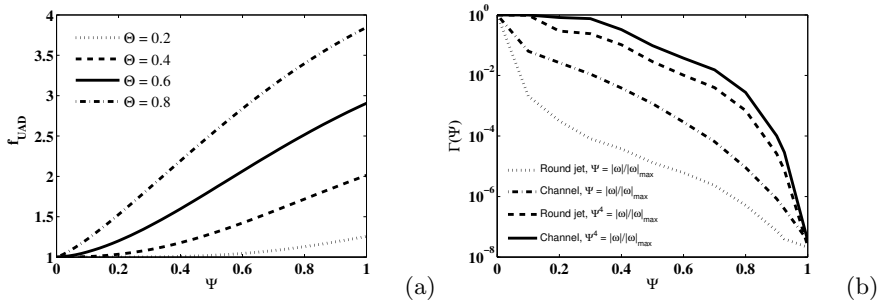

Fig. 1. Algebraic f_{UAD} function (a) and Volume pdf integrated from Ψ to 1 (b).

3 Applications and results

The approach described in section 2.3 has been tested on two different test cases, the plane channel flow and the round jet flow. Five different hexahedral structured grids, in the following named from 1 to 5, have been used to test the sensitiveness of the UAD approach to different resolutions.
As we followed the definition of geometric Δ proposed by Deardorff [1], we decided to build up the grids applying an isotropic coarsening between each one and the subsequent with a constant ratio $\sqrt{2}$, starting from a first grid able to well-resolve the flow field. Considering that grid 1 is the starting grid, its is quite simple to observe that grid 5 presents cells with the geometric Δ 4 times larger. Details regarding each test case grids are reported in the next sections. The time step for the simulations has been set constant and has been chosen to guarantee a Courant number lesser than 0.5; as the time step has a filtering effect over the solution, it has been scaled in the same way the physical dimensions have been coarsened.
The simulations have been performed on a finite volume solver in Gaussian

C_{UAD}	0	2	4	8	16	32

Table 1. C_{UAD} constants used in the preliminary analysis.

formulation using the Crank-Nicholson second order scheme in time and a centred second order scheme in space.
A first set of preliminary simulations have been carried out, combining the 4

models with 6 different values of the constant C_{UAD}, as in table 1. A response surface to value the quality of the results has been generated through the interpolation of the starting matrix using ordinary kriging [10] with the goal to find an optimum value for each model.
A second set of simulations has then been performed, combining the 4 different models with the 5 computational grids. As in the preliminary case, a response surface has been generated interpolating the resulting matrix with ordinary kriging to describe the behaviour of the cost function F:

$$F = 0.5\varepsilon_U + 0.25\varepsilon_d + 0.25\varepsilon_s \tag{4}$$

$$\varepsilon_U = \int_V \frac{(U_{LES} - U_{DNS})^2}{U_{DNS}^2} dV \tag{5}$$

$$\varepsilon_d = \sqrt[3]{\varepsilon_{uu} \cdot \varepsilon_{vv} \cdot \varepsilon_{ww}} \tag{6}$$

$$\varepsilon_s = \sqrt{\varepsilon_{uv} \cdot \varepsilon_{uw}} \tag{7}$$

$$\varepsilon_{ij} = \int_V \frac{(R_{ij}^{LES} - R_{ij}^{DNS})^2}{(R_{ij}^{DNS})^2} dV \tag{8}$$

where U is the time averaged streamwise velocity and R_{ij} represents the generic component of the Reynolds stress tensor.
The main concern about kriging application was the definition of a consistent length scale regarding the constant, the models and the grids. First of all, in each analysis the length scale has been set equal for both axes, as to get *square matrices*, then we defined different partitions for each parameter. When dealing with the models, the length scale has been equally divided while when dealing with the constant it has been linearly divided with the constant value. The same approach has been conserved for the parameter set on the grid length scale, which has been divided linearly with the coarsening ratio.

Plane Channel Flow

The results of the simulations in a plane channel flow at $Re_\tau = 395$ are here illustrated.The computations were carried out on structured grids with constant spacing in the streamwise and spanwise direction and hyperbolic spacing in the wall-normal direction. The ratio between contiguous cells volumes is always lesser than 1.1 and it tends towards the unity approaching the wall. The main characteristics of the grids are presented in table 2. In the present analysis, the x axis is coincident with the streamwise direction, the y axis with the wall-normal direction, the z axis with the spanwise direction and the computational domain is taken equal to $2\pi h \; x \; 2h \; x \; \pi h$, being h the channel half-width.
As clear from the data in the table, not all the grids are able to capture the necessary scales to correctly simulate the flow at the wall: since our research activity aimed at checking how error behaves more than trying to reduce the error, we decided to strictly keep the concept of isotropically coarsening the

grid even in the wall-normal direction.
The one-equation and the Smagorinsky model do not behave correctly approaching at the wall, as ν_{LES} doesn't correctly scale: for this reason, the models have been corrected with the addition of a Van Driest damping term.

Grid	nr of cells	Δx^+	Δy^+	Δz^+
1	80 X 100 X 100	30	$1.5 \rightarrow 15$	12
2	56 X 70 X 70	42.5	$2.1 \rightarrow 21$	17
3	40 X 50 X 50	60	$3 \rightarrow 30$	24
4	28 X 35 X 35	85	$4.2 \rightarrow 42$	34
5	20 X 25 X 25	120	$6 \rightarrow 60$	48

Table 2. Main characteristics of the grids used for the Plane Channel Flow case.

The results are compared with the DNS data by Kim [11] and the statistical moments contributing to the definition of the cost function F have been normalised over the computed u_τ.
Two series of simulations have been carried out; in the first one both the convective and the diffusive term were discretised with centred second-order schemes, while in the second one they were discretised with a centred fourth-order scheme. Both sets of preliminary simulations where performed on grid 3 to limit the computational resources needed.
Figure 2 shows the cost function F isocontours normalised in each row by the value of F at $C_{UAD} = 0$. The application of UAD in combination with the Van Driest damping deteriorates the quality of the results, and the phenomenon gets worse increasing the value of C_{UAD}: this is probably due to the fact that the beneficial effect that the Van Driest damping performs combined to the model, which imposes a decrease of $\bar{\Delta}$ towards the wall, is counteracted by UAD which increases the $\bar{\Delta}$ dimensions in the boundary layer. This behaviour is connected to a sensible deterioration in u_τ predictions for the model corrected with the Van Driest Damping.A sensible reduction of the error is instead observed for both the discretisation schemes when UAD is combined with variational multi-scale model, while WALE produces more accurate results only when second-order schemes are used. These results may be justified by the fact that in the variational multiscale-approach the model acts only over the small scales, while the WALE model acts on all the flow scales: a high value of the constant C_{UAD} combined with a high order scheme makes the model error to mask completely the smaller numerical error.
The optimum value for the constant C_{UAD} has been chosen through a minimum analysis of the cost function, represented by the dotted line in figure 2 (a) and (b): as the best value of C_{UAD} for the models corrected with the Van Driest damping is actually 0, we anyway set a symbolic value of 1 as, although we expect that the results will be worst than without the application of UAD, it is of a certain interest to test the stability of the error when $\bar{\Delta}$ is modified.

Following the optimum C_{UAD} value definition for each model, a database of

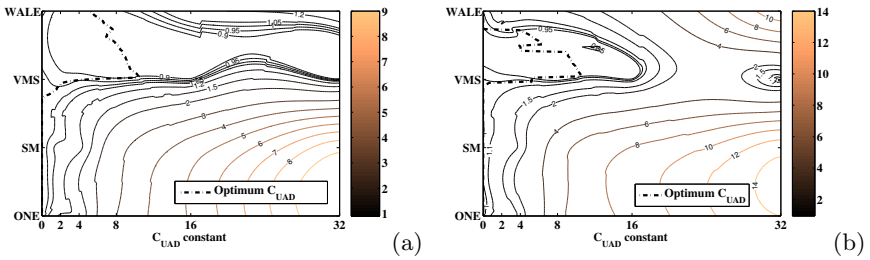

Fig. 2. F response surface on grid 3 using second (a) and fourth (b) order schemes.

simulations has been generated crossing the model applied and the grid resolution. The same database has been replicated without the anisotropic filter and furthermore a set of coarse DNS has been simulated too, for a result of 45 simulations for each of the discretisation schemes used.
The u_τ response surface resulting from second order *traditional* LES database is presented in fig. 3 (a): the data, normalised on the u_τ value computed by Kim [11], look quite similar for all the models and deteriorate as the grid coarsens. Models used in combination with the Van Driest damping produce slightly more accurate results as scale resolution decreases when compared to the other models or coarse DNS. UAD approach combined with the optimum constant didn't perturb significantly u_τ predictions, while the fourth order scheme application produces more accurate results as shown in fig. 3 (b).
In picture 4 the cost function F normalised with the corresponding values

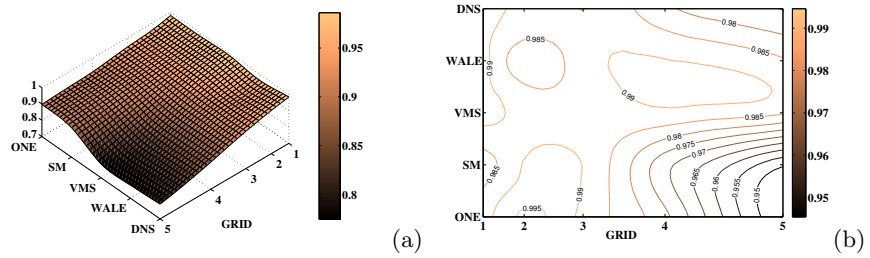

Fig. 3. second order u_τ response surface (a) and u_τ ratio between second and fourth order prediction (b).

computed through standard LES is presented. The most interesting result is a quite good consistency for the "*refined*" part of the response surface, meaning that the approach is actually able to adapt itself through the variation of

the global shape parameter Θ to the correct level of smoothing. Conversely, the main problem emerging from this analysis is indeed that the behaviour becomes quite unpredictable when UAD is combined with coarse grids and it's arguable if this happens for a poor resolution of the boundary layer or if the approach does not work properly in presence of a large numerical error.

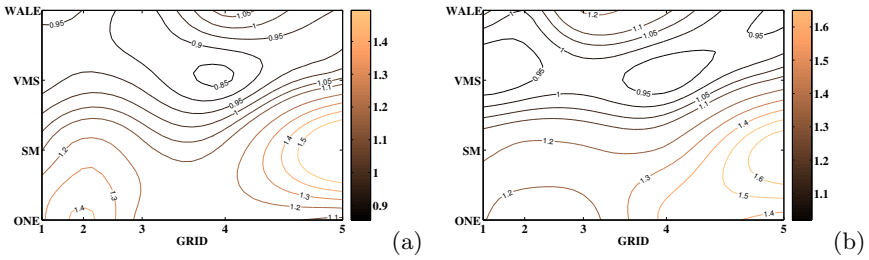

Fig. 4. error response surface of UAD LES compared to traditional LES for second order (a) and fourth order (b) accuracy.

Round Jet Flow

In this section, the results of the analysis carried out on a round jet flow test case are presented. A maximum Reynolds number, referenced to the peak of the mean streamwise velocity profile and the initial jet diameter, up to $Re_D = 21000$, has been considered. The computations have been performed on five different structured grids, on the same regular domain defined by $[0, 15D] \times [-5.5D, 5.5D] \times [-5.5D, 5.5D]$, the most refined one being discretised as the finest grid of Sagaut and Lê [12]. The discretisation on each cross section (y, z planes in Table 3) along the streamwise direction has been kept constant in the jet zone, while gaussian-shaped coarsening has been applied outwards. Along the streamwise direction x, a constant increment has been applied, while the dimension of the first cell layer has been chosen in order to comply with the advice in [13, 14]. More details are summarised in table 3.
As far as the jet inlet boundary surface is concerned, particular attention has been paid to the correct setting of the velocity profile: a flat, $1m/s$ streamwise velocity profile has been imposed outwards the jet region, while inside a hyperbolic-tangent function [13] has been set:

$$\frac{u\,(r)}{U_{ref}} = \frac{1}{2}\left(1 - \tanh\left[\frac{r_{jet}}{4\theta_{jet}}\left\{\frac{r}{r_{jet}} - \frac{r_{jet}}{r}\right\}\right]\right). \tag{9}$$

Moreover, a white-noise-spectrum turbulent fluctuation has been imposed on the whole inlet surface reference velocity field, adding up to, respectively, 4%

Grid	nr of cells	Jet zone $\Delta y = \Delta z$	Outwards $\Delta y = \Delta z$	Jet inlet Δx	Outlet Δx
1	100 X 120 X 120	$D/36$	$1.00D$	$D/16$	$0.3D$
2	70 X 85 X 85	$D/25$	$1.15D$	$D/12$	$0.4D$
3	50 X 60 X 60	$D/18$	$1.35D$	$D/8$	$0.6D$
4	35 X 42 X 42	$D/13$	$1.60D$	$D/6$	$0.85D$
5	25 X 30 X 30	$D/9$	$1.90D$	$D/4$	$1.2D$

Table 3. Main characteristics of the grids used for the Round Jet case.

along the x axis and 0.1% in the radial directions, in agreement with the tabulated experimental data [15].

The results of the computations have been compared with detailed experimental data from the Ercoftac Database [15]. Since the test case doesn't present a periodic behaviour in the streamwise direction, the cost function F has been evaluated as the mean value of the cost functions defined on four yz planes at $x/D = 0.2; 2.0; 4.0; 8.0$ respectively.

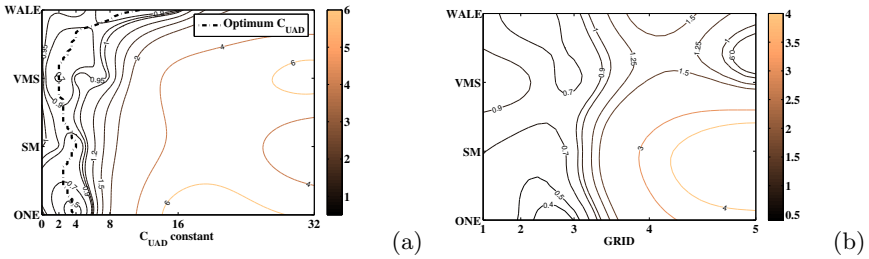

Fig. 5. F response surface on grid 3 (a) and on the five grids with optimum C_{UAD} values (b) for the Round Jet test case.

Figure 5 (a) shows the response surface of the cost function F on grid 3, crossing the four models and the six C_{UAD} values previously introduced, and normalised as in section 3. The thick dotted line identifies the optimum value of C_{UAD} on the response surface, depending on the model chosen. From the figure, the reduction in cost function F due to UAD is strong for each of the models, and approaches 30% and 50% circa, for the variational multi-scale and the one-equation models, respectively. Another interesting feature is that the optimum value of C_{UAD} seems to be quite independent on the model chosen, and anyway it is generally included in the $[2, 4]$ range. The only slightly different behaviour is seen for the coupling of UAD with the WALE model, where the optimum is reached at $C_{UAD} = 12$ circa; nevertheless, in this case the behaviour of UAD is much more straight along the C_{UAD} range, and a reduction in F by approximately 10% can be achieved even for it being in the optimum range identified for the other models. Lastly, the UAD performance

then deteriorates as C_{UAD} increases to values greater than eight.
The behaviour of the error cost function F on each grid, obtained setting the optimum C_{UAD} value for each of the models considered, has been reconstructed through kriging and plotted in figure 5 (b), normalised with respect to *traditional* LES. As it appears from the response surface, the application of UAD produces a stable global error reduction as the grid is refined; the total reduction in cost function adding up to more than 50% on the plain LES value. On the other side, a drawback of the UAD seems that, the approach unpredictably affects the results on coarse grids, as – even if in a framework of increasing error for each of the models – it appears much more stable when in presence of VMS or WALE, while instead the normalised cost function rapidly climbs up to values greater than 4 when adopting the one-equation and the Smagorinsky models.

4 Concluding Remarks

A local extension of the subfilter wavelength $\bar{\Delta}$ in LES has been investigated. Different grid resolutions, models and discretisation schemes have been considered on two well established test cases and the results have been compared to DNS/experimental data. The analysis of the error cost function stresses how this approach is beneficial for shear flows and can be effective even for wall-bounded flows, if the model can correctly scale ν_{LES} at the wall. The approach looks able to adapt itself to produce adequate wavelength extension when dealing with reasonable physical resolution, while it leads to unpredictable results when applied to really coarse grids: as a high Θ induces a strong effect even at low Ψ values, probably the large scales of motion come to be affected by UAD at low resolution.

References

1. J.W. Deardorff, Journal of Fluid Mechanics **41**, 453-465 (1970).
2. J. Bardina, J.H. Ferziger, W.C. Reynolds, AIAA Paper 80-1357 (1980).
3. J.C. Magnient, P. Sagaut, M. Deville, Physics of Fluids **13**, 1440-1449 (2001).
4. S. Ghosal, Journal of Computational Physics **125**, 187-206 (1996).
5. A. Yoshizawa, Journal of the Physical Society of Japan, Vol. **54** (1985).
6. J. Smagorinsky, Monthly Weather Review **91**(3) 99-165 (1963).
7. T.J.R. Hughes, Physics of Fluids **13** (2), 505-512 (2001).
8. F. Nicoud, F. Ducros, Flow, Turbulence and Combustion **62**, 183-200 (1999).
9. P.J. Mason, N.S. Callen, Journal of Fluid Mechanics **162**, 439-462 (1986).
10. J.C. Jouhaud, P. Sagaut, Journal of Fluids Engineering **130** (2008).
11. J. Kim, P. Moin, R. Moser, Journal of Fluid Mechanics **177**, 133-166 (1987).
12. P.Sagaut, T.H. Lê, Direct and Large Eddy Simulation II, Kluwer, 81-92 (1997).
13. D.J. Bodony, PhD Thesis, Stanford University (2005).
14. P. Sagaut, Large-Eddy Simulation for Acoustics, Cambridge (2007).
15. F. Anselmet, L. Fulachier, ERCOFTAC database, Exp. C38 (1993).